ACS APPLIED MATERIALS & INTERFACES

Letter

www.acsami.org

Scalable Solid-Template Reduction for Designed Reduced Graphene Oxide Architectures

Jun Chen,*[,†] Roderick L. Shepherd,[‡] Joselito M. Razal,[†] Xiao Huang,[§] Weimin Zhang,[‡] Jie Zhao,[‡] Andrew T. Harris,[‡] Shu Wang,[#] Andrew I. Minett,[‡] and Hua Zhang*[,§]

[†]Intelligent Polymer Research Institute, Australian Institute for Innovative Materials, Innovation Campus, University of Wollongong, Wollongong, NSW, 2522, Australia

[‡]Laboratory for Sustainable Technology, School of Chemical and Biomolecular Engineering, University of Sydney, Sydney, NSW 2006, Australia

[§]School of Materials Science and Engineering, Nanyang Technological University, Block N4.1, 50 Nanyang Avenue, Singapore 639798

[#]Institute of Chemistry, Chinese Academy of Sciences, No. 2 North first Street, Haidian Distinct, Beijing, 100190, China

Supporting Information

ABSTRACT: Herein, we report a solid-state reduction process (in contrast to solution-based approach) by using an environmentally friendly reductant, such as vitamin C (denoted VC), to be directly employed to solid-state graphene oxide (GO) templates to give the highly active rGO architecture with a sheet resistance of as low as 10 Ω sq^{-1}. In addition, predesigned rGO patterns/tracks with tunable resistivity can be directly "written" on a preprepared solid GO film via the inkjet-printing technique using VC/H_2O as the printing-ink. This advanced reduction process allows foreign active materials to be preincorporated into the GO matrix to form quality active composite architectures.

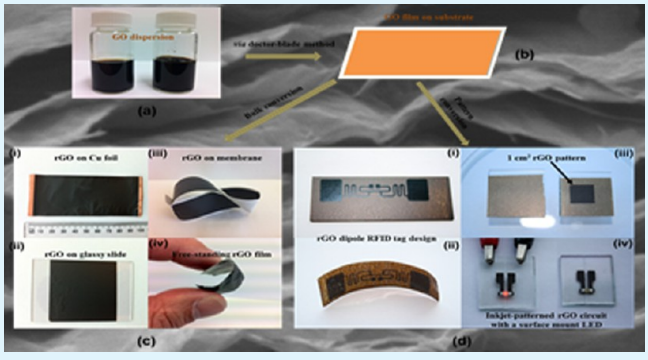

KEYWORDS: *graphene oxide, solid-state reduction, reduced graphene oxide, vitamin C, inkjet printing*

Graphene and reduced graphene oxide (rGO) are expected to show wide applications because of their unique 2D structures and remarkable physical and chemical properties.[1−5] The mechanical exfoliation[6] and chemical vapor deposition (CVD)[7] are widely used for production of high-quality, crystalline graphene sheets. However, the applicability of these two methods is limited by the difficulty in reproducibility and massive production of graphene.

To overcome the aforementioned limits, researchers have employed solution-based chemical approaches, in which the graphene oxide (GO) is reduced to obtain the reduced graphene oxide (rGO).[8,9] The rGO-based materials are broadly used for various applications, including electronic devices,[10−14] sensors,[15−19] electrochemical energy storage and conversion,[20−22] etc. Traditional solution-based approaches could result in the restacking of rGO sheets, which limits the utilization and decreases the performance of rGO-based materials in device applications. To overcome the restacking of rGO, various chemical reduction approaches have been explored, such as the solution-based[23−26] or vapor-based[27] treatment with hydrazine, electrochemical reduction,[28−30] thermal annealing,[31] and combinations of these techniques.[32] However, all these methods mentioned above not only showed disadvantages, such as difficulty of scaling-up, not environmentally friendly, high cost, etc., but also exhibited limits in the applicability of different substrates, which are critical for design and fabrication of devices for further applications.

In this work, we report an advanced processing protocol to prepare active rGO and rGO composite architectures via a solid-state reduction approach (in contrast to solution-based method[33−36]), which could be directly applied to preprepared GO templates deposited on different substrates (both rigid and flexible) for various devices. In addition, the predesigned active rGO patterns/tracks with variable resistance via taking the advantage of inkjet printing technique using VC solution as the ink to be directly "written" onto the solid GO templates, as well as the introduction of additional active components into the GO matrix to produce high-quality multifunctional rGO-based composite architectures, are also achieved.[37]

Figure 1 shows a schematic illustration of typical solid-state reduction processes for both bulk conversion and designed pattern conversion. First, a modified Hummers method[38] was used to obtain the purified aqueous GO dispersion (0.5 wt %). Then, a stable GO slurry (Figure 1a) with concentration of up

Received: May 31, 2013
Accepted: June 22, 2013
Published: June 22, 2013

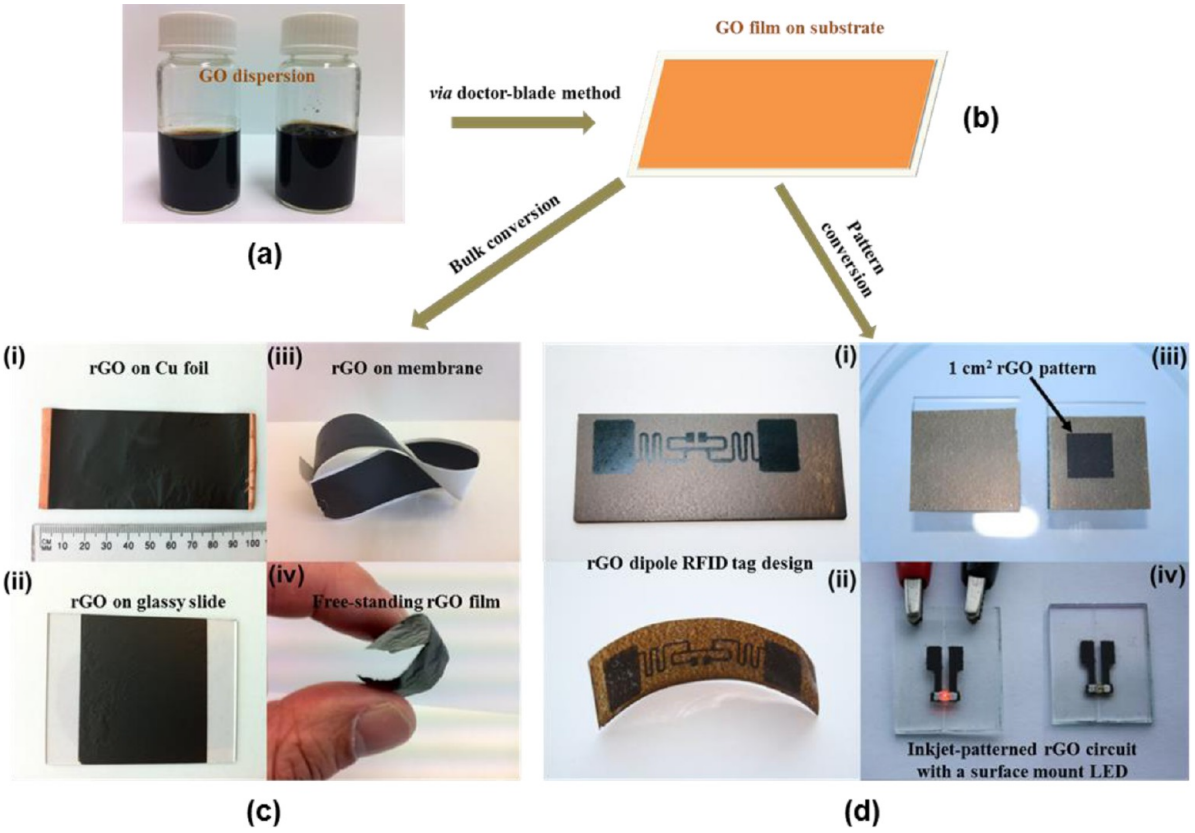

Figure 1. Solid-state reduction process for the preparation of rGO architectures. (a) Slurry-style GO dispersion. (b) GO film coated onto a substrate via the doctor-blade method. (c) Bulk conversion approach for preparation of rGO on different substrates: (i) Cu foil, (ii) glassy slide, (iii) PVDF membrane; (iv) free-standing rGO film peeled off from glassy slide substrate. (d) Pattern conversion for preparation of rGO via inkjet printing: (i,ii) rGO dipole RFID tag design before (i) and after (ii) tape lift-off; (iii) GO coated on glass (left), converted rGO pattern (right); (iv) inkjet-printed rGO circuit with a surface mount LED affixed with silver paint. The ITO glass substrate is used.

to 3 wt % was used as the precursor material and coated onto various rigid and flexible substrates including copper foil, glass, polyester (PET) sheet and polyvinylidene difluoride (PVDF) membrane via the doctor-blade method (Figure 1b and Figure S1 in the Supporting Information). Herein, two reduction protocols have been developed and employed to convert the GO to rGO (Figure 1c, d) in solid-state reduction process. First, to convert the entire GO film to rGO (referred to as bulk conversion, Figure 1c), the GO-coated substrate was immersed into a concentrated vitamin C (denoted VC, an environmentally friendly reductant) solution. This reduction was manifested by a color change of the film from brown (GO) to black (rGO). The rGO sheet resistivity could be tuned from ~1 kOhm sq^{-1} (2 S cm^{-1}) for the partially reduced GO film, referred to as prGO, to ~10 Ohm sq^{-1} (~200 S cm^{-1}) for the highly reduced GO film, referred to as hrGO, via the control of VC concentration and the incubation time. Furthermore, by using the VC solution as the Ink in an inkjet printer and the GO film as the "paper", a conductive rGO pattern was created on a substrate (referred to as pattern conversion). From both the bulk and pattern conversion strategies, free-standing rGO architectures could be obtained (Figure 1c, d). The pattern conversion strategy, in particular, is able to produce any predesigned rGO patterns/tracks, as demonstrated by a rGO dipole radio frequency identification (RFID) tag (Figure 1d(i, ii), or a rGO circuit providing electronic connection to light a light-emitting diode (LED) in Figure 1d(iv).

The cross-section SEM images of as-prepared rGO films in Figure 2a and Figure S2 in the Supporting Information revealed a corrugated surface morphology.[39] This intersheet corrugation prevented the rGO sheets from completely restacking, resulting in the formation of macroporous expanded film structure. It is worth mentioning that such corrugated rGO structure, which was typically achievable via high-temperature treatment,[40] can be facilely realized by our novel-designed one-step solid-state reduction protocol.

The reduction process of GO was also monitored by X-ray photoelectron spectroscopy (XPS), X-ray diffraction (XRD), and Raman spectroscopy. Figure 2b shows the C1s region of the XPS spectra for the GO, prGO and hrGO. The C1s region for GO shows two distinct peaks at 285.0 and 287.2 eV, corresponding to the sp^2 carbon and C−O single-bond components, respectively, and a small peak at 289.1 eV, corresponding to the C═O double-bond components.[41] The C:O ratio of 3.3:1 for GO was obtained, which is in agreement with the previous report.[42] In the prGO and hrGO spectra, the spectral difference in the peak intensity reflects the level of chemical reduction. The C:O ratio of 5.4:1 was obtained for prGO. Compared to GO, the increase in C:O ratio in prGO suggests a considerable deoxygenation via the VC reduction process.[43] The further reduction, as seen in the hrGO spectrum, led to a further increase in the C:O ratio (9.5:1), indicating the further removal of the oxygenated species. In addition, the sheet resistance of the hrGO film is ~200 S cm^{-1},

dx.doi.org/10.1021/am402084y | ACS Appl. Mater. Interfaces 2013, 5, 7676−7681

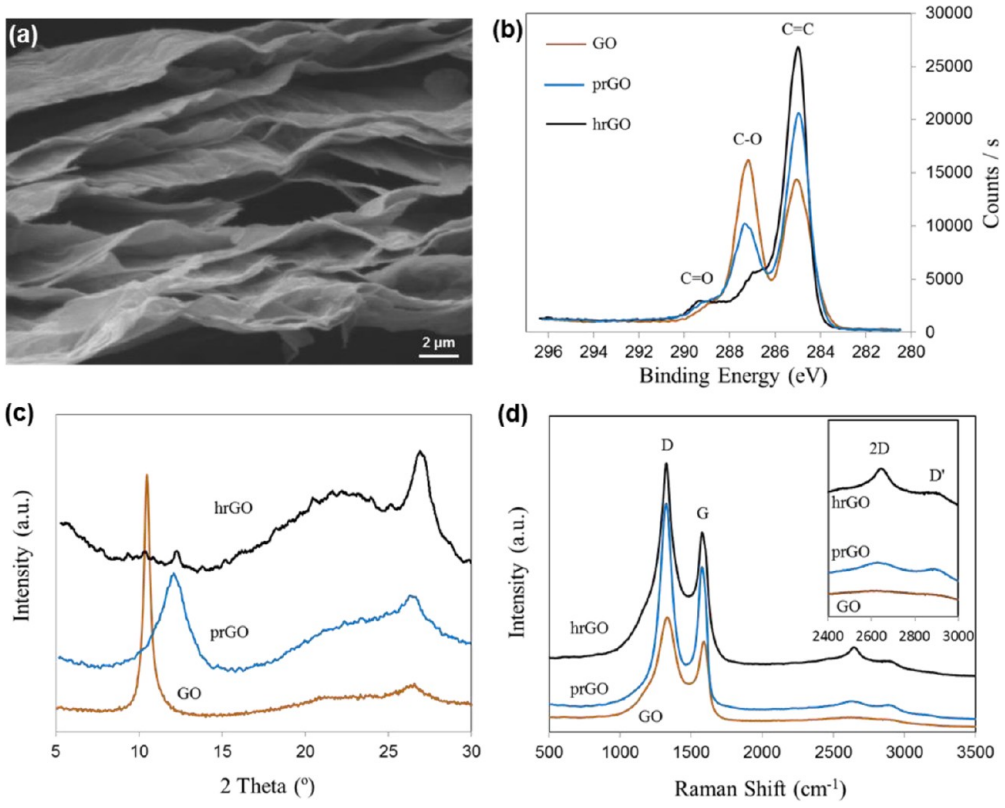

Figure 2. (a) SEM image of the cross section of a typical rGO film. (b) XPS C1s spectra of as-prepared GO, prGO and hrGO films. (c) XRD patterns of as-prepared GO, prGO and hrGO films. (d) Raman spectra obtained at laser wavelength of 633 nm showing the D, G, 2D, and D′ bands of the GO, prGO and hrGO films. Inset: Enlarged view of the 2D and D′ bands.

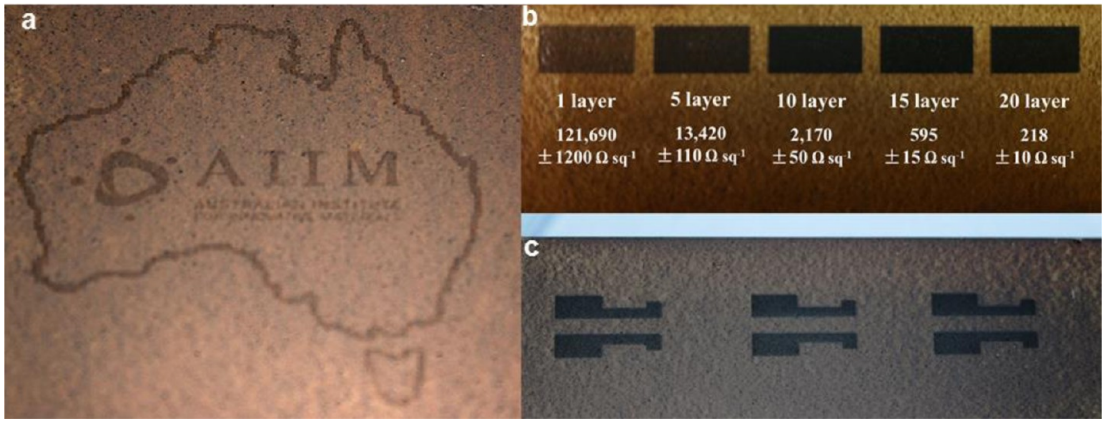

Figure 3. Samples of designed rGO tracks via inkjet printing approach using VC solution as the green reduction ink. Digital photographs of (a) rGO track – Australia map, (b) rectangular rGO patterns with various sheet resistivity as a function of the number of printed ink layers, and (c) a design of rGO tracks/patterns.

which is highly conductive and comparable with the reported highly reduced GO.[25,28]

XRD analysis was carried out to study the crystal structure of the GO, prGO, and hrGO films (Figure 2c). The pattern of the initial GO film showed a major peak at $2\theta = 10.5°$ ($d = 0.803$ nm), indicating a larger interlayer spacing compared with that of graphite due to the oxygen functional groups.[44] Upon reduction, the XRD pattern changed considerably. For the prGO film which was obtained when GO was immersed into 0.5 M VC solution for 2 h, the peak originally located at 10.5° shifted to 12.5° ($d = 0.707$ nm), while the peak at $2\theta = 26.9°$ ($d = 0.330$ nm) sharpened with an increase in intensity, which is related to the pristine graphene sheet structure.[44] As for the XRD pattern of hrGO, the intensity of the peak at 12.5° further decreased, and the shoulder in the 18.1–25.0° ($d = 0.492$–0.356 nm) region centered at 21.9° ($d = 0.4035$ nm) and the peak at 26.9° ($d = 0.328$ nm) have intensified. These characteristic peaks observed for hrGO commensurate with those observed for previously reported rGO in the literature.[41] The remaining broad shoulder from 18.1° ($d = 0.492$ nm) to 25.0° ($d = 0.356$ nm) indicates that the rGO film has a disordered layered structure, which is consistent with the corrugated structure shown in the SEM images (see Figure S2 in the Supporting Information).

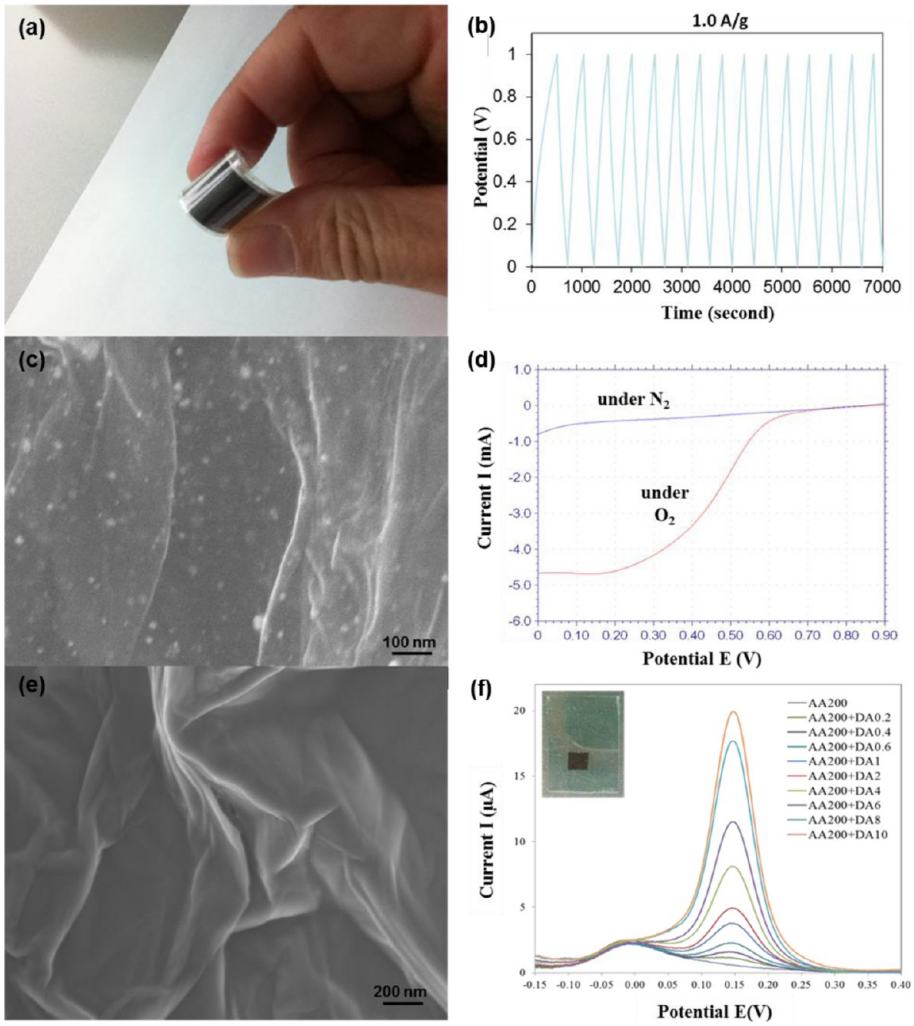

Figure 4. (a) Optical image of a flexible supercapacitor device made from rGO thin films. (b) Typical galvanostatic charge/discharge curves of the representative rGO film supercapacitor at 1.0 A g^{-1}. (c) SEM image of an rGO/PtNPs composite film. (d) Linear sweep voltammgram of catalytic ORR reaction using the rGO/PtNPs composite film in 0.5 M H_2SO_4 solution. (e) SEM image of an rGO/Nafion composite film. (f) DPV of different DA concentration from 0 to 10 mM in the presence of 200 mM AA using rGO/Nafion composite film in pH 7.0 PBS. Inset: photo of rGO/Nafion on ITO glass.

The reduction of GO was also confirmed by the Raman spectra. Figure 2d gives three characteristic peaks of GO at 1327, 1590, and 2628 cm^{-1}, associated with the D, G, and 2D bands, respectively.[45] The 2D band of GO film is very weak, whereas the prGO and hrGO give the higher intensity of the 2D band (the inset in Figure 2d), which increases substantially with the increased level of GO reduction, because of the enlarged sp^2 domains in rGO and the partial restoration of the graphitic crystalline lattice.[46] In addition, after reduction of GO, the G peak shifted toward lower wave numbers (1580 cm^{-1} for prGO and 1576 cm^{-1} for hrGO) compared to that of GO (1590 cm^{-1}), much closer to that of graphite (1570 cm^{-1}). The shifts are attributed to the recovery of hexagonal network of carbon atoms with defects, which are consistent with the previous report.[1,47]

Different from the conventional solution-based reduction of GO,[10,11,24] the aforementioned novel reduction process with VC solution as the green reduction Ink, for the first time, provides a great opportunity for the generation of predesigned conductive rGO patterns/tracks via inkjet printing approach to promote the applications of rGO-based devices. As shown in Figure 3, a designed rGO pattern (Australian map) was produced by this approach. By controlling inkjet-printing parameters, such as the drop spacing and the number of printed layers, rGO patterns with tunable resistivity can be generated. Figure 3b displays a series of rGO patterns with different printed layers of VC Ink. The obtained average sheet resistances of the rGO patterns are ca. 121 690 ± 1200, 13 420 ± 110, 2170 ± 50, 595 ± 15, and 218 ± 10 Ω sq^{-1} for 1, 5, 10, 15, and 20 printed VC Ink layers, respectively. This strategy represents a very important step in advancing the electronics industry. According to the use of aqueous solution as the reduction ink, hence virtually any standard commercial inkjet printer could be used for this process. In addition, combined with the facile selective lift-off process, this unique approach not only allows the patterned rGO features to be removed from the original substrate to form free-standing structures with tag designs (Figures S3 and S4 in the Supporting Information) but also can selectively remove the unconverted GO regions and leave the rGO pattern on the substrate for designed electronic devices (see Figures S5 and S6 in the Supporting Information).

To illustrate the application of rGO architectures, we fabricated a flexible, sandwiched, symmetric capacitor cell (Figure 4a and Figure S7 in the Supporting Information) via

assembling a symmetric membrane electrode, in which two identical pieces of the as-prepared rGO-coated PVDF membranes (rGO/PVDF) were attached back-to-back. Then, the membrane electrode was sandwiched in between two ITO-coated PET sheets (30 Ω sq^{-1}), in which the PVDF and ITO layer acted as the separator and current collector, respectively. After the as-assembled capacitor was backfilled with a degassed aqueous electrolyte (1.0 M Na_2SO_4) (Figure 4a), it was evaluated at a constant galvanostatic charge−discharge rate of 1.0 A g^{-1} (Figure 4b). It exhibits a stable specific capacitance of 160.2 F g^{-1} with a high energy density of 26.1 W h kg^{-1}.

An in situ reduction process with VC was utilized for the simultaneous reduction of GO and Pt^{4+} precursor to obtain Pt nanoparticles (PtNPs) decorated rGO film (referred to as PtNPs/rGO), which was confirmed by SEM (Figure 4c) and XRD analysis (see Figure S8 in the Supporting Information). The PtNPs/rGO composite was then used for the electrocatalytic oxygen reduction reaction (ORR) (Figure 4d). The linear sweep voltammograms of the PtNPs/rGO composite electrode showed a substantial catalytic oxygen reduction reaction with an onset potential of ca. +0.61 V (vs. Ag/AgCl) in an oxygen-saturated 0.5 M H_2SO_4 solution. It indicates that the as-prepared PtNPs/rGO has an electrocatalytic activity toward the ORR reaction.

Besides rGO-metal NP composites, our patterned reduction procedure can also be used for the facile preparation of patterned rGO/Nafion film as an example to demonstrate the fabrication of electrochemical biosensors, because rGO is a biocatalytically active element for electroanalytical sensing of various biomolecules, such as dopamine (DA).[48] As shown in Figure 4e, a patterned thin film of rGO(90 wt %)/Nafion(10 wt %) onto an ITO-coated glass (the inset in Figure 4f) was used for the direct detection of DA by differential pulse voltammetry (DPV) in phosphate buffered saline (PBS) solution (pH 7.0). The DPV curves show clear peak responses associated with the oxidation of DA, exhibiting good selectivity for DA in the presence of high concentration (200 μM) of ascorbic acid (Figure 4f and Figure S9 in the Supporting Information). These results suggest that the rGO/Nafion thin film is one kind of promising electrode materials for the direct detection of DA. It is envisaged that this process to prepare rGO/polymer composites will be used in development of electrode architectures with active interfaces for various applications.

In conclusion, we have demonstrated a simple and effective green chemical reduction approach to create highly conductive and active rGO and rGO-based composite architectures. Furthermore, the patterned rGO structures with tunable resistances are obtained via the control of reduction parameters. This simple process is amenable to a range of printing techniques including the inkjet, roll-to-roll, reel-to-reel, flexo-, and gravure printing. We believe that our method will open up an avenue for the realization of graphene applications.

■ ASSOCIATED CONTENT

Supporting Information

Full information on methods and preparation procedures, and detailed results and discussion for individual applications. This material is available free of charge via the Internet at http://pubs.acs.org.

■ AUTHOR INFORMATION

Corresponding Author

*E-mail: junc@uow.edu.au.

Notes

The authors declare no competing financial interest.

■ ACKNOWLEDGMENTS

J.C., R.L.S., J.M.R., A.I.M., and A.T.H. thank the Australian Research Council, the University of Wollongong, and the University of Sydney for ongoing financial support and AIIM for critical support; A.I.M. and A.T.H. thank the University of Sydney's ACMM, and S.W. thanks the ICCAS and Chinese National Science Foundation. H.Z. thanks Singapore MOE for support under AcRF Tier 2 (ARC 10/10, No. MOE2010-T2-1-060), AcRF Tier 1 (2012-T1-001-161), Start-Up Grant (M4080865.070.706022), Singapore National Research Foundation under the Campus for Research Excellence and Technological Enterprise (CREATE) programme.

■ REFERENCES

(1) Edo, G.; Chowalla, M. *Adv. Mater.* **2010**, *22*, 2392−2415.
(2) Huang, X.; Qi, X. Y.; Boey, F.; Zhang, H. *Chem. Soc. Rev.* **2012**, *41*, 666−686.
(3) Huang, X.; Yin, Z. Y.; Wu, S. X.; Qi, X. Y.; He, Q. Y.; Zhang, Q. C.; Yan, Q. Y.; Boey, F.; Zhang, H. *Small* **2011**, *7*, 1876−1902.
(4) Chhowalla, M.; Shin, H. S.; Eda, G.; Li, L. J.; Loh, K.; Zhang, H. *Nat. Chem.* **2013**, DOI: 10.1038/nchem.1589.
(5) Huang, X., Zeng, Z. Y., Zhang, H., *Chem. Soc. Rev.*, **2013**, *42*, 1934-1946 (2013).
(6) Hernandez, Y.; Nicolosi, V.; Lotya, M.; Blighe, F. M.; Sun, Z.; De, S.; McGovern, I. T.; Holland, B.; Byrne, M.; Gun'Ko, Y. K.; Boland, J. J.; Niraj, P.; Duesberg, G.; Krishnamurthy, S.; Goodhue, R.; Hutchison, J.; Scardaci, V.; Ferrari, A. C.; Coleman, J. N. *Nat. Nanotechnol.* **2008**, *3*, 563.
(7) Li, X.; Cai, W.; An, J.; Kim, S.; Nah, J.; Yang, D.; Piner, R.; Velamakanni, A.; Jung, I.; Tutuc, E.; Banerjee, S. K.; Colombo, L.; Ruoff, R. S. *Science* **2009**, *324*, 1312.
(8) Loh, K. P.; Bao, Q.; Eda, G.; Chhowalla, M. *Nature Chem.* **2010**, *2*, 1015−1024.
(9) Park, S.; Ruoff, R. S. *Nat. Nano.* **2010**, *4*, 217−224.
(10) Wang, S.; Pu, J.; Chan, D. S. H.; Cho, B. J.; Loh, K. P. *Appl. Phys. Lett.* **2010**, *96*, 143109.
(11) He, C. L.; Zhuge, F.; Zhou, X. F.; Li, M.; Zhou, G. C.; Liu, Y. W.; Wang, J. Z.; Chen, B.; Su, W. J.; Liu, Z. P.; Wu, Y. H.; Cui, P.; Li, R. W. *Appl. Phys. Lett.* **2009**, *95*, 232101.
(12) Huang, X.; Zeng, Z. Y.; Fan, Z. X.; Liu, J. Q.; Zhang, H. *Adv. Mater.* **2012**, *24*, 5979−6004.
(13) Liu, J. Q.; Yin, Z. Y.; Cao, X. H.; Zhao, F.; Wang, L. H.; Huang, W.; Zhang, H. *Adv. Mater.* **2013**, *25*, 233−238.
(14) Li, B.; Cao, X. H.; Ong, H. G.; Cheah, J. W.; Zhou, X. Z.; Yin, Z. Y.; Li, H.; Wang, J. L.; Boey, F.; Huang, W.; Zhang, H. *Adv. Mater.* **2010**, *22*, 3058−3061.
(15) Dong, X.; Shi, Y.; Huang, W.; Chen, P.; Li, L. J. *Adv. Mater.* **2010**, *22*, 1649.
(16) Ohno, Y.; Maehashi, K.; Yamashiro, Y.; Matsumoto, K. *Nano Lett.* **2009**, *9*, 3318.
(17) Lim, C. X.; Hoh, H. Y.; Ang, P. K.; Loh, K. P. *Anal. Chem.* **2010**, *82*, 7387.
(18) Agarwal, S.; Zhou, X. Z.; Ye, F.; He, Q. Y.; Chen, G. C. K.; Soo, J.; Boey, F.; Zhang, H.; Chen, P. *Langmuir* **2010**, *26*, 2244.
(19) He, Q. Y.; Wu, S. X.; Yin, Z. Y.; Zhang, H. *Chem. Sci.* **2012**, *3*, 1764−1772.
(20) Stoller, M. D.; Park, S.; Zhu, Y.; An, J.; Ruoff, R. S. *Nano Lett.* **2008**, *8*, 3498−3502.
(21) An, X.; Simmons, T.; Shah, R.; Wolfe, C.; Lewis, K. M.; Washington, M.; Nayak, S. K.; Talapatra, S.; Kar, S. *Nano Lett.* **2010**, *10*, 4295−4301.
(22) Wang, X.; Zhi, L. J.; Mullen, K. *Nano Lett.* **2008**, *8*, 323.
(23) Gilje, S.; Han, S.; Wang, M.; Wang, K. L.; Kaner, R. B. *Nano Lett.* **2007**, *7*, 3394.

(24) Gao, W.; Alemany, L. B.; Ci, L.; Ajayan, P. M. *Nat. Chem.* **2009**, *1*, 403.
(25) Becerill, H. A.; Mao, J.; Liu, Z.; Stoltenberg, R. M.; Bao, Z.; Chen, Y. *ACS Nano* **2008**, *2*, 463.
(26) Yamaguchi, H.; Eda, G.; Mattevi, C.; Kim, H.; Chhowalla, M. *ACS Nano* **2010**, *4* (1), 524−528.
(27) Eda, G.; Fanchini, G.; Chhowalla, M. *Nat. Nanotechnol.* **2008**, *3*, 270−274.
(28) Zhou, M.; Wang, Y.; Zhai, Y.; Zhai, J.; Ren, W.; Wang, F.; Dong, S. *Chem.—Eur. J.* **2009**, *15*, 6116−6120.
(29) Li, X.; Zhang, G.; Bai, X.; Sun, X.; Wang, X.; Wang, E.; Dai, H. *Nat. Nanotechnol.* **2008**, *3*, 538−542.
(30) Wang, Z. J.; Zhou, X. Z.; Zhang, J.; Boey, F.; Zhang, H. *J. Phys. Chem. C* **2009**, *113*, 14071−14075.
(31) Becerril, H. A.; Mao, J.; Liu, Z.; Stoletenberg, R. M.; Bao, Z.; Chen, Y. *ACS Nano* **2008**, *2*, 463−470.
(32) Tung, V. C.; Allen, M. J.; Yang, Y.; Kaner, R. B. *Nat. Nanotechnol.* **2009**, *4*, 25−29.
(33) Yin, Z. Y.; Wu, S. X.; Zhou, X. Z.; Huang, X.; Zhang, Q. C.; Boey, F.; Zhang, H. *Small* **2010**, *6*, 307−312.
(34) Dua, V.; Surwade, S. P.; Ammu, S.; Agnihotra, S. R.; Jain, S.; Roberts, K. E.; Park, S.; Ruoff, R. S.; Manohar, S. K. *Angew. Chem., Int. Ed.* **2010**, *49*, 2154−2157.
(35) Zhang, J.; Yang, H.; Shen, G.; Cheng, P.; Zhang, J.; GuoS.. *Chem. Commun.* **2010**, *46*, 1112−1114.
(36) Fernández-Merino, M. J.; Guardia, L.; Paredes, J. I.; Villar-Rodil, S.; Solís-Fernández, P.; Martínez-Alonso, A.; Tascón, J. M. D. *J. Phys. Chem. C* **2010**, *114* (14), 6426−6432.
(37) Chen, J.; Shepherd, R. L.; Razal, J.; Minett, A. I. Australian Provision Patent No. 35 114 062, lodged on Sept 19, 2011.
(38) Dikin, D,A.; Stankovich, S.; Zimney, E. J.; Piner, R. D.; Dommett, G. H. B.; Evmenenko, G.; Nguyen, S. T.; Ruoff, R. S. *Nature* **2007**, *448*, 457.
(39) Qiu, L.; Zhang, X. H.; Yang, W. R.; Wang, Y. F.; Simon, G. P.; Li, D. *Chem. Commun* **2011**, *47*, 5810−5812.
(40) Niu, Z.; Chen, J.; Hng, H. H.; Ma, J.; Chen, X. *Adv. Mater.* **2012**, *24*, 4144−4150.
(41) Park, S.; An, J.; Potts, J. R.; Velamakanni, A.; Murali, S.; Ruoff, R. S. *Carbon* **2011**, *49*, 3019−3023.
(42) Mattevi, C.; Eda, G.; Agnoli, S.; Miller, S.; Mkhoyan, K. A.; Celik, O.; Granozzi, G.; Garfunkel, E.; Chhowalla, M. *Adv. Funct. Mater.* **2009**, *19*, 1−7.
(43) Stankovich, S.; Piner, R. D.; Chen, X.; Wu, N.; Nguyen, S. T.; Ruoff, R. S. *J Mater Chem.* **2006**, *16* (2), 155−8.
(44) Buchsteiner, A.; Lerf, A.; Pieper, J. *J Phys Chem B.* **2006**, *110*, 22328−22338.
(45) Dong, X. C.; Fu, D. L.; Fang, W. J.; Shi, Y. M.; Chen, P.; Li, L. J. *Small* **2009**, *5*, 1422−1426.
(46) Dong, X. C.; Su, C. Y.; Zhang, W. J.; Zhao, J. W.; Ling, Q. D.; Huang, W.; Chen, P.; Li, L. Z. *Phys. Chem. Chem. Phys.* **2010**, *12*, 2164−2169.
(47) Tung, V. C.; Allen, M. J.; Yang, Y.; Kaner, R. B. *Nat. Nanotechnol.* **2009**, *4*, 25−29.
(48) Shang, N.g.; Papakonstantinou, P.; McMullan, M.; Chu, M.; Stamboulis, A.; Potenza, A.; Dhesi, S. S.; Marchetto, H. *Adv. Funct. Mater.* **2008**, *18*, 3506−3514.